Introducing the Renewable Energy Network Optimization Tool (ReNOT): Part I.

Randall Alliss, Robert Link, Duane Apling, Michael Mason, Heather Kiley,
Kremena Darmenova, Glenn Higgins
Northrop Grumman Information Systems
3975 Virginia Mallory Drive
Chantilly, VA

ABSTRACT

As the renewable energy industry continues to grow so does the requirement for atmospheric modeling and analysis tools to maximize both wind and solar power. Renewable energy generation is variable however; presenting challenges for electrical grid operation and requires a variety of measures to adequately firm power. These measures include the production of non-renewable generation during times when renewables are not available. One strategy for minimizing the variability of renewable energy production is site diversity. Assuming that a network of renewable energy systems feed a common electrical grid, site diversity ensures that when one system on the network has a reduction in generation others on the same grid make up the difference. This paper introduces the Renewable Energy Network Optimization Tool (ReNOT) a disruptive technology used to maximize useable power and minimize intermittency of that power through site diversity.

Keywords: Renewable Energy, wind-on-wind power, site optimization

1. INTRODUCTION

As the renewable energy industry continues to grow so does the requirement for atmospheric modeling and analysis tools to maximize both wind and solar power. Renewable energy generation is variable however; presenting challenges for electrical grid operation and requires a variety of measures to adequately firm power. These measures include the production of non-renewable generation during times when renewables are not available. One strategy for minimizing the variability of renewable energy production is site diversity. Assuming that a network of renewable energy systems feed a common electrical grid, site diversity ensures that when one system on the network has a reduction in generation others on the same grid make up the difference.

A similar problem faces government organizations interested in space to ground laser communications. Clouds severely attenuate a free space optical communication (FSOC) signal therefore in order to achieve maximum link performance one must use site diversity techniques to find optimal ground stations. We have developed and applied the Lasercom Network Optimization Tool (LNOT) modeling system to perform site selection and availability trade studies. This has been accomplished through the development of a fifteen year climatological and high resolution cloud database based on geostationary satellite imagery.

The site-diversity strategy we developed for laser communications is used to mitigate the intermittency in alternative energy production systems while still maximizing saleable energy. Recently, LNOT has been adapted to optimally site potential wind turbine and solar collector farms. The adapted system is referred to as the Renewable Energy Network Optimization Tool (ReNOT). Although the problem is different than for FSOC, the modeling framework is easily extendable. The new system has a plug-in architecture that allows us to accommodate a wide variety of renewable energy system designs and performance metrics. For example, one might optimize site locations to maximize day ahead predictable power all the while accounting for short term variability.

In this paper we describe several aspects of the ReNOT capability including the datasets used (both solar and wind), the optimization algorithm as well as the scoring algorithm. In an accompanying paper we illustrate several case studies of both wind and photovoltaic (P/V) farm deployment.

2. DATA SETS USED IN RENOT

The cloud database required to run ReNOT have been developed originally for the FSOC problem. Fifteen years of GOES imagery over the Continental United States and Hawaii have been run through a custom cloud retrieval algorithm to provide cloud properties at 4km horizontal and 15 minute temporal resolution, respectively. Cloud analyses from the NOAA GOES imager data are derived using the algorithms described by Alliss et al.[1] The GOES imager has 5 bands: visible (0.6 µm), shortwave infrared (3.9 µm) (SWIR), water vapor (6.7 µm), longwave infrared (10.7 µm) (LWIR), and split window (11.2 µm). The water vapor channel, is not used for cloud detection and is replaced by a multispectral fog product at night, and a shortwave reflectivity product during the day. The resolution of the visible band is 1 km, and the other bands are at 4 km. In the cloud detection algorithms the 1 km data is resampled to 4 km so that it may be readily combined with the data from the other bands.

Our existing high-resolution cloud cover database is coupled with a sophisticated solar irradiance model[2,3] to provide the basic databases needed for the site selection of solar energy farms.

In addition, we use the Weather Research and Forecasting Model (WRF) to develop a climatological wind database. Below is a brief description of the cloud retrieval algorithm as well as the wind database development.

2.1 CLEAR SKY BACKGROUND

The cloud algorithms use threshold tests to determine the prescense of clouds and require knowledge of a clear sky backgroun (CSB). The CSB is the radiation received by the GOES sensor in the absence of clouds. This background can be reflected, emitted, or a combination of both. The reflective and emissive properties of the ground vary from place to place; therefore, using fixed thresholds in the cloud tests will produce faulty cloud decisions in some places. For example, an albedo threshold tuned to detect clouds over "typical" terrain will consistently produce spurious clouds over the highly reflective surface of White Sands, NM. Similarly, seasonal variations in ground temperature will affect the LWIR background. Terrain height, soil moisture, and illumination angle also affect the CSB. In order to account for these differences the CSB must be modeled separately for each pixel at each time.[3]

In order to minimize the effects of diurnal cycles, the CSB is processed using data from the previous 30 days at a single analysis time (e.g., 1200 UTC). This scheme isolates most of the diurnal variation in temperature and illumination. A separate CSB is calculated for each band or multispectral product in use at the particular analysis time: LWIR, visible, reflectivity product, and fog product.

The albedo CSB is the average of the darkest ten percent of albedo values from the previous 30 days for the pixel being analyzed. The 30-day data window represents a compromise between making the sample large enough to be likely to include several clear observations and making the sample small enough to be sensitive to seasonal variations.

The reflectivity CSB is calculated using the darkest ten percent of reflectivity product values from the previous 30 days. The calculation is in other respects similar to the calculation for the albedo CSB.

The fog product CSB is calculated by identifying the warmest 10 percent of LWIR values for the pixel over the previous 30 days. The fog product values for the selected times are averaged to form the fog product CSB. This procedure differs from the albedo and reflectivity versions (which choose clear pixels based on the albedo and reflectivity themselves) because both extremes of the fog product values indicate clouds.

The LWIR CSB is determined with the aid of the LWIR regression model, in which each pixel's LWIR temperature is estimated using a linear regression model. The regression model is populated with prototypical clear sky pixels from the entire analysis region. These prototypes are chosen using a series of tests that detect only pixels that have a high probability of being clear (i.e., even without the benefit of thresholds from the regression modeling they are clearly cloud-free.) We use the prototype pixels to fit coefficients of a linear regression model with twelve predictors, including pixel level data from the GOES imager, regional data from the NWS surface reports, time, and terrain.

The LWIR regression model is used to estimate the clear sky LWIR brightness temperature in each pixel. The differences between the regression model temperature and the measured GOES LWIR temperature are the LWIR residuals. The warmest ten percent of the LWIR residuals are averaged to obtain the LWIR residual CSB that is used in the LWIR cloud test.

2.2 CLOUD TESTS

All of the cloud tests are made by comparison to a dynamically computed CSB, described in the previous section.

The visible channel is used when the solar zenith angle is less than 89º; however, for solar zenith angles between 89º and 81º cloud detections in this band are deweighted, due to the low signal-to-noise ratio when the scene is illuminated at low solar elevations. If the calculated albedo exceeds the CSB by a predefined threshold the pixel is deemed cloudy. Conversely, if the albedo is less than the CSB by more than the threshold, the pixel is deemed clear (i.e., cloud detections from other tests may be negated).

The LWIR is used directly in a cloud detection test, in addition to being used in the multispectral tests. A pixel is considered cloudy if the LWIR CSB for the pixel exceeds the LWIR temperature by a predefined threshold. Unlike the visible and multispectral tests, the LWIR test is usable at any time of day.

The fog product is calculated as the difference between the LWIR and SWIR brightness temperatures.[4] The emissivity of water clouds in the SWIR is lower than in the LWIR; therefore, low clouds produce colder SWIR temperatures, resulting in $T_{\mathrm{LW}} - T_{\mathrm{SW}} \gtrsim 2\mathrm{K}$.[4] (The exact threshold is determined by the clear-sky background model described below.) This product can detect clouds that have LWIR temperatures too similar to the ground temperature to be detected by the LWIR alone. The fog product is also useful for detecting high ice clouds. These clouds are transmissive and therefore appear warmer in the SWIR, resulting in $T_{\mathrm{LW}} - T_{\mathrm{SW}} \lesssim 5\mathrm{K}$.[4] Because the SWIR is dominated by reflected radiation during the day, the fog product is usable only at night.

The shortwave reflectivity product is calculated by subtracting the thermal component from the SWIR, leaving only the reflected solar component.[4,5] Because water clouds are highly reflective in the SWIR, while ice is poorly reflective in the SWIR, the reflectivity product can readily distinguish between low clouds and snow cover. Absent the reflectivity product, the visible channel could misidentify the latter as cloud.

2.3 EXAMPLE CLOUD ANALYSES

Figure (1a,b) below shows an example of the fifteen, thirteen cloud climatology over the Continental United States and Hawaii, respectively. The climatology indicates the well known pattern of couds including the relatively clear Southwest US and the more persistent cloud Pacific Northwest and Great Lakes regions. Over Hawaii, the peaks of Mauna Kea, Mauna Loa, and Haleakala all show the characteristic minimum in clouds. In addition, mesoscale features such as the Kona Plume and the local sea-breeze fronts along the Kona coast are evident in their local maximum in cloudiness.

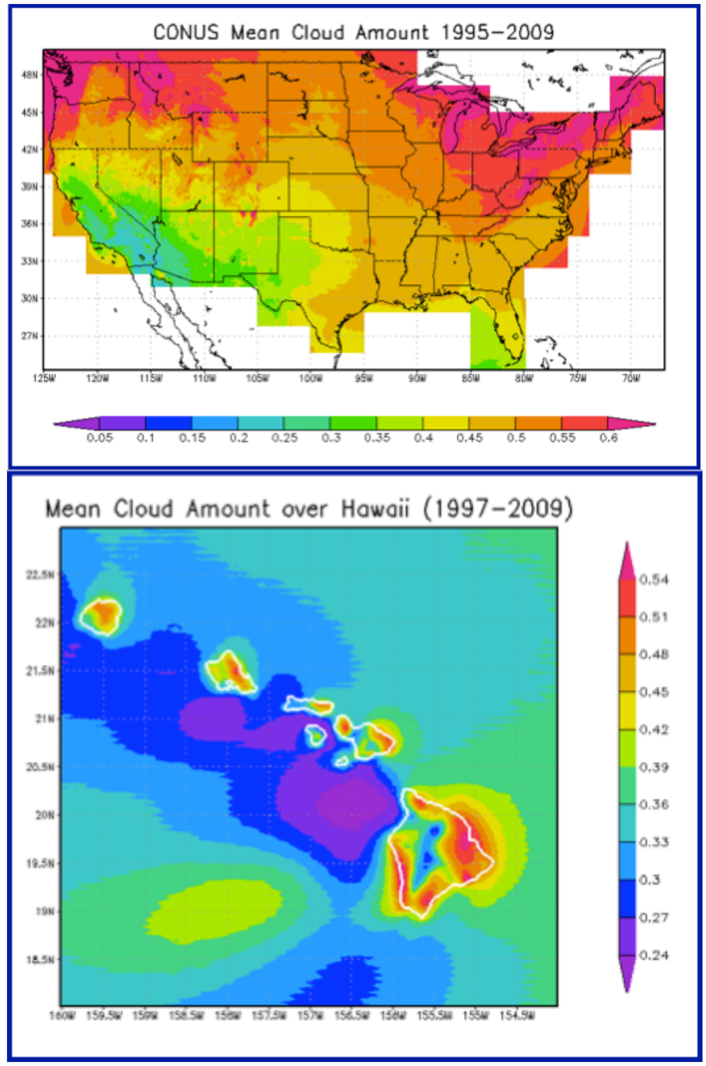

Figure 1a: Mean cloud occurrence over CONUS between 1995-2009. (b) same but for Hawaii.

Because this database has a temporal resolution of 15 minutes the cloud correlations between sites and in time can be explicity calculated instead of inferred. The cloud database has been validated against whole sky imager (WSI) over a nine month period as well as pyrheliometer data at multiple locations throughout the United States. Results indicated an excellent agreement between the two datasets. Comparisons were also made to data from the Desoto photovoltaic farm located in Florida[8]. Correlations between the database were approximately 0.7.

2.4 THE WIND DATABASE

The Weather Research and Forecasting (WRF) mesoscale model is applied to generate high-resolution wind databases to support the site selection of wind farms. These databases are generated on High Performance

Computing systems such as the Rocky Mountain Supercomputing Center (RMSC). WRF is a high resolution, limited area, non-hydrostatic model. We successfully performed decadal simulations with WRF, running in climate mode, for current and future periods over CONUS. We utilized a number of features implemented in the WRF model that allow realistic representation of the climate system in long-term simulations, e.g. variable CO_2 concentrations, diurnal variations of the skin Sea Surface Temperature (SST), deep soil temperature and SST updates. The NCEP reanalysis and the ECHAM5/MPI-OM General Circulation Model (GCM) are used as the forcing model which provide the necessary initial and boundary conditions. For the present climate (1995- 2009), WRF was forced with NCEP reanalysis data. For the 21th century climate, we used an ECHAM5 simulation with the Special Report on Emissions (SRES) A1B emissions scenario. WRF was run in nested mode at spatial resolution of 108 km, 36 km and 12 km and 28 vertical levels. The wind speed at approximately 40 meters height (hub-height for most wind turbines) is saved every hour. In this study the Single-moment 5-class (WSM5) microphysics scheme and the Kain-Fritsch convective parameterization scheme is utilized. The Noah Land Surface Model and Yonsei University (YSU) Planetary Boundary Layer scheme are used. Shortwave and longwave radiation are computed with the CAM SW and LW scheme.

Comparisons of model output are made to data collected from a wind farm in Montana and show correlations around 0.7. In addition, comparisons were made to wind datasets obtained from the National Renewable Energy Lab (NREL) website (*http://www.nrel.gov/wind/integrationdatasets/western/data.html*). Wind speed data were downloaded for four locations nearest the cooresponding WRF grid points for the period 2004-2006. The NREL dataset is valid at 100 meters AGL and 1 arc-minute spatial and 10 minute temporal resolution, respectively. The data were aggregated so they could be more easily compared to our dataset which is valid at 12km and 1 hour resolution. Results for the four sites are shown in table 1 below.

It should be stated that although we have high confidence in the quality of these databases the ReNOT tool has been designed in such a way to accommodate any other cloud or wind database. The only requirement is that the database contain a time series of the parameters of interest and not simply the means over time of the parameters. This way the correlation between sites can be explicity resolved in the optimization. In addition, the dataset is required to be gridded spatially. This then makes it possible to substitute the users of choice preferred dataset. This make ReNOT essentially agnostic to the data used for site selection.

Correlations between NREL wind data and RENOT wind data from 2004-2006	
Site 1	0.68
Site 2	0.61
Site 3	0.68
Site 4	0.70

Table 1: Correlations between the NREL Western Wind dataset and that developed for this project. Correlations are relatively high given the differences in resolution.

3. MODELING AND OPTIMIZATION APPROACH

In order to translate the cloud data into information useful for computing the incoming solar radiation we use a sophisticated solar model and statistics of cloud height/thickness to compute direct and indirect insolation. Insolation is computed using a multi-layer radiative transfer model[2,3]. The orientation geometry of the solar panels is modeled directly from design specifications of an installed panel systems (i.e., SunPower T0 panels) with a pointing algorithm. In addition, panel-to-panel shadowing is accounted for in the solar calculation. The solar model was empirically fit to the aggregate power generation data provided from Nov and Dec 2009 Desoto data[8].

An algorithm for finding an optimal network of renewable energy generating stations faces two competing goals. First, it must search efficiently through the configuration space by using information gleaned from networks evaluated earlier in the process to guide the search toward even better networks. Second, it must avoid getting trapped in locally optimal solutions, which, though better than other nearby candidates, are inferior to configurations more distant in the configuration space. These goals conflict because using a lot of information from previous evaluations necessarily restricts us to a more local search. Conversely, searching more broadly through the configuration space precludes us from taking advantage of what we have discovered about previous configurations we have evaluated. We strike a balance between these conflicting goals by adopting some strategies from genetic algorithms, which provide a systematic way of starting out with a broad search early in the calculation and narrowing in to a more local search as the calculation progresses.

Each iteration of the renot algorithm begins by identifying a pool of eligible stations. All of the new networks examined in the iteration will have stations drawn from this pool. The number of stations that remain in the pool from one iteration to the next determines how broad or focused the search will be. Replacing all or most of the stations results in a broader search; replacing only a few results in a more focused search. In the parlance of genetic algorithms, the station pool represents the gene pool, and the fraction of stations replaced at each iteration represents the mutation rate. Stations are selected for the pool using a quasi-random number generator, instead of the more traditional pseudo-random number generator. This innovation allows us to sample the stations more uniformly across the geographical area of interest, taking advantage of our intuition that the best networks will be geographically diverse.

Once the station pool is in place we create networks to evaluate by drawing stations randomly from the pool. Currently, we enforce non-duplication in these station draws, but one could also allow duplicates as a way of representing stations with unequal nameplate capacities (i.e., a station appearing twice in a network represents a single station with twice the capacity of a baseline station). All of the stations so generated are evaluated and ranked against each other and against the stations evaluated in previous iterations. The stations appearing in the top few networks (of all time, not just this iteration) are marked to be kept in the next iteration, and the remainder will be replaced.

The exact number of stations to be kept in the pool from one iteration to the next varies throughout the calculation according to a schedule chosen at the beginning of the calculation. Initially, we keep only the stations in the best network. As the calculation progresses we keep more and more stations until eventually only a single station is being retained. Thereafter we begin to reduce the size of the station pool, still replacing only a single station at each iteration. By the end of the calculation, the pool is just one station larger than the network size, and we are keeping all but a single station. Thus, we proceed from a very broad search, in which we are selecting a lot of new stations at random in every iteration, to a very narrow search, in which we are keeping the best network we have seen so far and generating new networks by replacing individual stations.

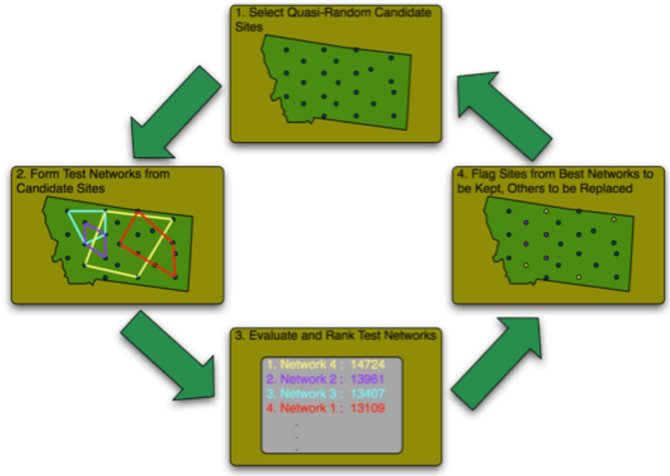

Figure 2: The ReNOT optimization process takes place in four discrete steps.

A typical optimization run evaluates the power generation on the order of 10^9 networks of wind and/or solar farms. These calculations make several simplifying assumptions in order to speed up the individual availability calculations. Once the optimization algorithm has identified a small number (10–20) of candidate networks, a more comprehensive evaluation is performed for each network. This evaluation includes a detailed calculation of power generation, both raw and useable as well as statistics of ramping events.

4. SCORING METRICS

Any optimization problem requires a scoring metric in order to evaluate networks of wind and/or solar farms.
ReNOT uses a scoring metric which optimizes on *useable power.* Useable power is our estimate of that amount of power that can be reliablly counted on by minimizing impacts of curtailment as well as the dependency on weather forecasts of wind and clouds. In this case curtailment represents an approxoimation to the excess power that can not be sold on market and therefore has to be dumped. This would be due to short-term fluctuations in power generation over the course of an hour, for example. The other consideration is the reliance on weather prediction. Prediction reflects the ability to forecast tomorrow's power generation. In general, networks with little curtailment and that produce more consistent, non-varying power day after day will be favored. Below we define three scoring metrics for wind (M1,M2,M3) and for solar (S1,S2,S3). The M3 and S3 metrics define the optimization metric referred to as *useable power*.

Wind specific metrics:

Power from the station is the result of the solar or wind calculation for the location and time.

$$p_{ij} = \text{Power from station } i \text{ at time index } j$$

$i \in \{1 \ldots N\}$,

$$j \in \{1 \ldots T\}$$

Summation over all stations at time j is the network power

$$P_j = \sum_{i=1}^{N} p_{ij}$$

Maximum power generated by any station at time j over the network

$$Q_j = \max_{i=1,N}\{p_{ij}\}$$

In this case, the metric is designed to produce a network that narrows in on the single best location for power production, on the mean.

$$\text{M1} = \frac{1}{T}\sum_{j=1}^{T} P_j$$

In the case of M2, the metric is designed to produce a network that widens out to a maximally diverse network, even at the expense of very poor aggregate power.

$$\text{M2} = \frac{1}{T}\sum_{j=1}^{T} Q_j$$

The running minimum network sum-power over a trailing time window (K+1 steps wide).

$$R_j^K = \min_{k=0,K}\{P_{j-k}\}$$

The trailing H-step mean of the running K-step trailing minimum. This will be a proxy for a day-ahead forecast with H set to enough time-steps to cover 24 hours (In principal, this could be set to any time length).

$$\overline{R}_j^{H,K} = \frac{1}{H}\sum_{k=1}^{H} R_{j-k}^K$$

The M3 metric caps utility at no more than the previous day's average power, and accounts for time-to-time variability over a shorter window. Networks that consistently produce power from day to day and time to time will be favored.

$$\text{M3} = \frac{1}{T}\sum_{j=1}^{T} \min\left(R_j^K, \overline{R}_j^{H,K}\right)$$

The metrics, M1, M2, and M3 represent a basic set that should span the space for ReNOT testing. Refinements could include better representations of ramping costs, better day-ahead forecast proxies, and season/hourly weights by electrical demand.

Solar specific metrics:

The amount of power from the station that would be produced under a perfectly clear sky.

$$s_{ij} = \text{Clear sky power from station } i \text{ at time index } j$$

The sum of predicted power over all stations in the network:

$$S_j = \sum_{i=1}^{N} s_{ij}$$

Indicator flag for the network, showing whether it potentially produce power or not:

$$w_j = \begin{cases} 1 : S_j > 0 \\ 0 : S_j \le 0 \end{cases}$$

Fractional output level of the network is the fraction of the potential clear-sky power that is produced:

$$f_j = \begin{cases} \dfrac{P_j}{S_j} : S_j > 0 \\ 0 : S_j \le 0 \end{cases}$$

Minimum fractional power produced by the network over the trailing *K* time steps for those time when it could have produced power:

$$F_j^K = \min_{\substack{k=0,K \\ \{w_{j-k}=1\}}} \{f_{j-k}\}$$

The trailing H-step average of the minimum fractional power for those times when the network could have been producing power.

$$\overline{F}_j^{H,K} = \begin{cases} \dfrac{\sum_{k=1}^{H} F_{j-k}^K}{\sum_{k=1}^{H} w_{j-k}} & : \displaystyle\sum_{k=1}^{H} w_{j-k} > 0 \\ 0 & : \displaystyle\sum_{k=1}^{H} w_{j-k} \le 0 \end{cases}$$

The corresponding S3, solar metric caps utility at no more than the previous 24-hour average power fraction times the current clear-sky power potential, excluding times when the network cannot produce power, and accounts for time-to-time variability over a shorter window by using the lowest fractional power output over last K-steps at each time. Networks that consistently produce power from day to day and time to time will be favored.

$$S3 = \frac{1}{T}\sum_{j=1}^{T} \min\left(F_j^K, \overline{F}_j^{H,K}\right) S_j$$

The K-steps (e.g., four 15 minutes steps) trailing average assures that rapidly ramping power levels create a poor value, favoring short term steady power output. The 24 hour average is a proxy of a next day's forecasted power output, favoring networks with high day-to-day persistence accuracy, which reasonably implies a network with a better day-ahead forecastability.

A graphical illustration of the M3/S3 metric is shown in Figure 3.

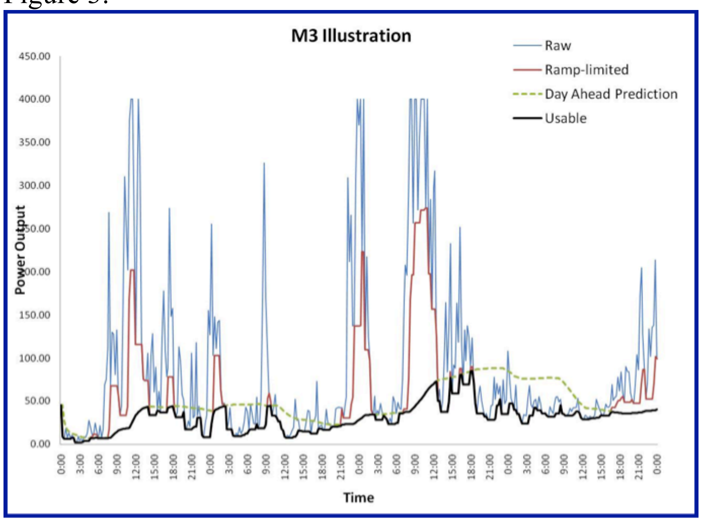

Figure 3: Illustration of the M3 metric.

The raw power of the network is shown by the blue line as a function of time. The short-term variability of power due to rapid fluctuations is shown in red (ramp-limited). The proxy for the day ahead prediction is given in the dash green line. The useable power is simply the minimum of the previous two (black line). In this case the useable power is that power which is limited by short-term curtailment and the ability to predict tomorrows generation. Networks with large Usable Power will be favored by the optimization.

The ReNOT tool can accommodate numerous constraints (e.g., number of sites, the geographic extent of the optimization, proximity to high-voltage transport lines, terrain constraints, population constraints). This capability is critical because of the practicalities of siting wind and/or solar farms. In some cases the optimal set of geographically diverse sites may not be practical due to issues stated above. If those constraints are factored in then a more reliable and defendable network can be found.

5. SUMMARY

The Renewable Energy Network Optimization Tool (ReNOT) has been developed to assist in the optimal placement of networks of wind and/or solar farms . ReNOT optimizes site selection to maximize usable power, by minimizing power intermittency and maximizing base load power of the system. It takes into consideration constraints on placement such as: location of transmission lines, population density, land costs and others. Use of this tool can assist in minimizing the conventional energy reserve requirements of the utility industry. In addition, ReNOT is a powerful tool that can assist policy makers, regulators, regional public stakeholders, transmission operators, and individual renewable operators and investors.

Finally, the development of high resolution regional climate simulations through dynamic downscaling is being performed to understand future wind, cloud, and temperature patterns and their impacts on existing and future renewable energy production capability. Running ReNOT on these future data sets allows us to select sites optimized for tomorrow's climate, rather than yesterday's. Part II of this paper will present case studies of both a wind and solar farm optimization.

ACKNOWLEDGMENTS

The authors wish to thank the Rocky Mountain Supercomputing Center (RMSC) for providing the compute cycles necessary to develop the historical and future climate wind databases as well as test runs of ReNOT.

REFERENCES

1. Alliss, R.J., M. E. Loftus, D. Apling, and J. Lefever, "The development of cloud retrieval algorithms applied to goes digital data," in *10th Conference on Satellite Meteorology and Oceanography*, pp. 330–333, American Meteorological Soc., January 2000.
2. Shapiro, R.,. 982: Solar Radiative Flux Calculations from Standard Surface Meteorological Observations.

SASC Scientific Report No. 1. AFGL-TR-82-0039;ADA118775

3. Shapiro, R., 1987: A simple Model for the Calculation of the Flux of Direct and Diffuse Solar Radiation Through the Atmosphere., STX Scientific Report No. 35. AFGL-TR-87-0200
4. Ellrod, G.P. "Advances in the detection and analysis of fog at night using goes multispectral infrared imagery," *Weather Forecasting* 10, pp. 606–619, 1995.
5. Lee, T.F., F. J. Turk, and K. Richardson, "Stratus and fog products using GOES-8 3.9 µm data," *Weather Forecasting* 12, pp. 664–677, 1997.
6. Allen, R.C., Jr., P. A. Durkee, and C. H. Wash, "Snow/cloud discrimination with multispectral satellite measurements," *J. Appl. Meteor*. 29, pp. 994–1004, 1990.
7. Setvak M. and C. A. Doswell, III, "The AVHRR channel 3 cloud top re.ectivity of convective storms," *Monthly Weather Review* 119, pp. 841–847, 1991.
8. Kankiewicz, A, Sengupta, M., and D. Moon. "Observed Impacts of Transient Clouds on Utility Scale PV Fields*,"* ASES SOLAR 2010 Conference Proceedings.